Mixed-Valence States of $[Fe_3O(CH_2XCO_2)_6(H_2O)_3]\cdot nH_2O$ (X = H, Cl, and Br) Characterized by X-ray Crystallography and ^{57}Fe-Mössbauer Spectroscopy¶

Takuma Sato,*,† Fumitoshi Ambe,† Kazutoyo Endo,‡ Motomi Katada,§,⊥ Haruka Maeda,† Tadahiro Nakamoto,§,⊥ and Hirotoshi Sano§,||

Contribution from The Institute of Physical and Chemical Research (RIKEN), Hirosawa, Wako-shi, Saitama 351-01, Japan, Showa College of Pharmaceutical Sciences, Higashi-tamagawagakuen, Machida, Tokyo 194, Japan, and Department of Chemistry, Faculty of Science, Tokyo Metropolitan University, Minami-ohsawa, Hachioji, Tokyo 192-03, Japan

Received September 5, 1995⊗

Abstract: Mixed-valence states of μ-oxo-centered trinuclear iron carboxylate complexes, $[Fe_3O(CH_2BrCO_2)_6(H_2O)_3]$ (**1**), $[Fe_3O(CH_3CO_2)_6(H_2O)_3]\cdot 2H_2O$ (**2**), and $[Fe_3O(CH_2ClCO_2)_6(H_2O)_3]\cdot 3H_2O$ (**3**), were characterized by X-ray crystallography and ^{57}Fe-Mössbauer spectroscopy. Compound **1** has a trapped-valence-type structure, i.e., one Fe(II)-type atom and two Fe(III)-type atoms. The central Fe_3O atoms construct nearly an isosceles triangle array with Fe−O bond distances of 1.86(1), 1.83(1), and 2.00(1) Å at 293 K. In the case of compound **2**, the X-ray structure shows good equivalence in geometry around the three iron atoms. Results of X-ray crystallography of **1** and **2** are consistent with the results of Mössbauer spectroscopy. The Mössbauer spectra of **1** show a trapped-valence state below 296 K. The Mössbauer spectra of compound **2** are simulated using a three-site relaxation model where an increased rate of intramolecular electron transfer is assumed among the three iron atoms with an increase in temperature. Black crystals of **3** were converted to red powders of $[Fe_3O(CH_2ClCO_2)_6(H_2O)_3]$ (**4**) due to loss of all three crystal water molecules when kept in air at ambient temperature. Mössbauer spectra of the dehydrated compound **4** show a temperature-independent trapped-valence state. On the other hand, there are three quadrupole doublets in the Mössbauer spectrum of the hydrated compound **3** measured at 86 K, one of which was ascribed to an Fe^{II} state and the remaining two to an Fe^{III} (Fe^{IIIA} and Fe^{IIIB}) state. It is found that two of the three doublets (Fe^{II} and Fe^{IIIA}) converge without appreciable line broadening with an increase in temperature, while the other doublet (Fe^{IIIB}) remains unchanged, indicating valence delocalization over the two iron atoms. The X-ray structure of compound **3** also indicates that valence delocalization takes place only between two iron atoms. At 112 K the central Fe_3O atoms array with the Fe−O bond distances of 2.003(2) (Fe1), 1.853(2) (Fe2), and 1.849(2) Å (Fe3). A temperature increase to 293 K changes the bond distances to 1.957(3) (Fe1) and to 1.895(3) Å (Fe2), while the bond distance of Fe3−O is almost unchanged (1.846(3) Å). There are intra- and intermolecular hydrogen bonds formed by the crystal water and coordinated water molecules in compound **3**. The results suggest that hydrogen-bonding interaction affects the local environment of iron atoms and induces valence delocalization between the two iron atoms.

Introduction

A number of mixed-valence trinuclear iron carboxylate complexes with the general formula of $[Fe^{II}Fe_2^{III}O(R-CO_2)_6(L)_3]\cdot nS$ are known in a variety of carboxylate ligands $R-CO_2$, monodentate ligands L, and solvate molecules S.[1] Three iron atoms are bridged by the oxygen atom located at the center of an iron triangle and also by the six carboxylate ligands in the circumference. Much attention has been paid to the electronic interactions among the three iron atoms via bridging ligands, and molecular symmetry has been studied in connection with intramolecular electron transfer and with optical and magnetic properties. X-ray crystal structures show that some of the complexes have a crystallographically imposed 3-fold axis through the central oxygen atom. Such crystal structures have been reported for a series of acetate−(pyridine derivative) complexes (R = CH_3, L = pyridine or its derivatives) and for the cyanoacetate−aqua complex (R = CH_2CN L = H_2O).[2−5] Temperature-dependent structural change has been reported for the acetate−pyridine complex (R = CH_3, S and L = pyridine). X-ray crystallography shows that this molecule exhibits a 32-site symmetry at 200 K; however, the 3-fold axis disappears at ∼190 K.[3] ^{57}Fe-Mössbauer spectroscopy of the acetate−pyridine complex shows a temperature-dependent trapped-to-averaged valence state. Above 190 K the valency is observed to be averaged with respect to the time scale of Mössbauer spectroscopy, while vibrational data indicate lower molecular symmetry

¶ Preliminary reports of the present study were published in the Proceedings of the RIKEN International Symposium on Unstable Nuclei and Particles as Probes in Physics and Chemistry (Saitama 1992) [*Hyperfine Interactions* **1994**, *84*, 559−562] and in the proceedings of the Eötvös Workshops in Science (Budapest 1994) [*J. Radioanal. Nucl. Chem.* **1995**, *190*, 257−261].

† The Institute of Physical and Chemical Research (RIKEN).

‡ Showa College of Pharmaceutical Sciences.

§ Tokyo Metropolitan University.

⊥ Current address: Radioisotope Research Center, Tokyo Metropolitan University, Minami-ohsawa Hachioji, Tokyo 192-03, Japan.

|| Current address: Department of Environmental Science, School of Social Information Studies, Otsuma Women's University, Karakida, Tama, Tokyo 206, Japan.

⊗ Abstract published in *Advance ACS Abstracts,* March 15, 1996.

(1) Cannon, R. D.; White, R. P. *Prog. Inorg. Chem.* **1988**, *36*, 195−298.

(2) Woehler, S. E.; Wittebort, R. J.; Oh, S. M.; Hendrickson, D. N.; Inniss, D.; Strouse, C. E. *J. Am. Chem. Soc.* **1986**, *108*, 2938−2946.

(3) Woehler, S. E.; Wittebort, R. J.; Oh, S. M.; Kanbara, T.; Hendrickson, D. N.; Inniss, D.; Strouse, C. E. *J. Am. Chem. Soc.* **1987**, *109*, 1063−1072.

(4) Jang, H. G.; Geib, S. J.; Kaneko, Y.; Nakano, M.; Sorai, M.; Rheingold, A. L.; Montez, B.; Hendrickson, D. N. *J. Am. Chem. Soc.* **1989**, *111*, 173−186.

(5) Nakamoto, T.; Katada, M.; Kawata, S.; Kitagawa, S.; Kikuchi, K.; Ikemoto, I.; Endo, K.; Sano, H. *Chem. Lett.* **1993**, 1463−1466.

0002-7863/96/1518-3450$12.00/0

corresponding to inequivalencies of the valence states even at room temperature with respect to the time scale of molecular vibrations.[2−4,6] Hendrickson et al. have proposed that the electron transfer occurs in the acetate−pyridine complex as an order−disorder phase transition associated with orientational disordering of the solvate molecule, based on the results of ^{57}Fe-Mössbauer and ^{2}H-NMR spectroscopies and heat capacity measurement.[3,7−11] The solvate pyridine molecule is located between the Fe_3O molecules with the molecular plane of the solvate pyridine molecule perpendicular to the Fe_3O plane. At temperatures below ∼150 K the solvate molecule is statically disordered, and in the temperature range of 170−190 K it begins to rotate dynamically around the *c*-axis. Incoherent neutron scattering measurement also indicates rotational motion of the solvate pyridine molecule.[12] Such dynamics of the solvate pyridine molecule is expected to induce a change in the potential-energy surface, which has one minimum at low temperatures to give three equivalent vibronic states. It has been reported that the magnetic exchange interaction between the three iron atoms in the acetate−pyridine complex is antiferromagnetic.[13] Recently Cannon et al. reported that there is also a significant intermolecular magnetic exchange interaction originating from the mixed valency at low temperatures (up to 50 K) in the acetate−pyridine complex.[14−17] The intermolecular magnetic exchange interaction splits spin states into low-lying manifolds and creates spin mixing.

The C_3-symmetric complexes have been reported only in a rhombohedral crystal system, while other complexes which have symmetries lower than C_3 have been reported in triclinic and monoclinic systems. Most of the lower symmetric complexes have no imposed symmetry and X-ray crystal structures show that the coordination geometries around iron atoms differ from each other to some extent.[7,18−20] Sorai et al. have reported thermochemical data for $[Fe_3O(CH_3CO_2)_6(3\text{-methylpyridine})_3]\cdot$3-methylpyridine which shows a temperature-dependent trapped-to-averaged valence state on Mössbauer spectra.[21] They interpreted the results by assuming different vibronic interactions for each pair of iron atoms; however, the differences seemed too small to be distinguished spectroscopically. The complex which has the most prominent inequivalency in terms of the coordination pattern was reported by Poganiuch et al. to be $[Fe_3O(CH_3CO_2)_6(TACN)]\cdot 2CHCl_3$ (TACN = 1,4,7-triazacyclononane), which shows a temperature-independent trapped-valence state on Mössbauer spectra.[22] One iron atom assigned to an Fe^{III} state has three nitrogen and three oxygen coordination atoms (N_3O_3) and the other two atoms assigned to an Fe^{III} and an Fe^{II} state are coordinated with O_6 atoms. In spite of the different coordination patterns of the two Fe^{III} atoms, Mössbauer spectra and temperature dependence of magnetic susceptibility could be resolved by assuming the same electronic conditions for the two Fe^{III} atoms.

Here we will report a unique example of the mixed-valence trinuclear iron chloroacetate complex, $[Fe_3O(CH_2ClCO_2)_6(H_2O)_3]\cdot 3H_2O$ (**3**), where the electronic state of each Fe^{III} atom is observed to be different in Mössbauer spectroscopy. Mössbauer spectra taken at various temperatures show that two distinct states, Fe^{IIIA} and Fe^{IIIB}, exist at low temperatures, and that valence delocalization takes place between only two iron atoms, Fe^{IIIA} and Fe^{II}, with increasing temperature. The valence state of each iron atom in **3** is defined by comparing the crystal structure of **3** with those of $[Fe_3O(CH_3CO_2)_6(H_2O)_3]\cdot 2H_2O$ (**2**) and $[Fe_3O(CH_2BrCO_2)_6(H_2O)_3]$ (**1**). X-ray crystallography of **3** shows the existence of intra- and intermolecular hydrogen bonds which may affect the electronic state of iron atoms.

Experimental Section

Materials. Synthetic procedures for compounds **1**, **2**, and **3** are essentially the same as the methods previously reported for mixed-valence iron carboxylate−aqua complexes.[6,23]

$[Fe_3O(CH_2BrCO_2)_6(H_2O)_3]$ (1): $FeCl_2\cdot 4H_2O$ (25 g, 0.125 mol), monobromoacetic acid (83.4 g, 0.6 mol), and sodium hydroxide (12 g, 0.3 mol) were dissolved in 350 mL of water. After allowing the solution to stand for several weeks, black crystalline precipitate was filtered and collected. Anal. Calcd for $C_{12}H_{18}Br_6Fe_3O_{16}$: C, 13.53; H, 1.70; Br, 45.01. Found: C, 15.12; H, 1.84; Br, 44.45.

$[Fe_3O(CH_3CO_2)_6(H_2O)_3]\cdot 2H_2O$ (2): $FeCl_2\cdot 4H_2O$ (10 g, 0.05 mol), sodium acetate (16.3 g, 0.12 mol), and acetic acid (30 g, 0.05 mol) were dissolved in 150 mL of water. The reaction mixture was allowed to stand for several weeks. Black crystalline precipitate was filtered and collected. Anal. Calcd for $C_{12}H_{22}Fe_3O_{18}$: C, 22.96; H, 4.50. Found: C, 23.62; H, 4.35.

$[Fe_3O(CH_2ClCO_2)_6(H_2O)_3]\cdot 3H_2O$ (3): Monochloroacetic acid (57 g, 0.6 mol) and sodium hydroxide (12 g, 0.3 mol) were dissolved in 150 mL of water. An aqueous solution of $FeCl_2\cdot 4H_2O$ (25.8 g, 0.13 mol) dissolved in 200 mL of water was added to the solution. The reaction mixture was allowed to stand for several weeks. Black crystalline precipitate was filtered and collected.

$[Fe_3O(CH_2ClCO_2)_6(H_2O)_3]$ (4): This compound was prepared by storing the hydrated compound **3** for several days under dry nitrogen. The hydrated complex **3** lost 6.3% of its original weight upon drying. This value shows excellent agreement with the calculated value (6.3%). Anal. Calcd for $C_{12}H_{18}Cl_6Fe_3O_{16}$: C, 14.34; H, 1.20; Cl, 42.33. Found: C, 14.07; H, 1.14; Cl, 41.89.

^{57}Fe-Mössbauer Spectroscopy. ^{57}Fe-Mössbauer spectra were determined by the conventional method of using a ^{57}Co−rhodium source moving in a constant-acceleration mode at room temperature against absorber samples kept in a cryostat at a desired temperature. ^{57}Fe-

(6) Meesuk, L.; Jayasooriya, U. A.; Cannon, R. D. *J. Am. Chem. Soc.* **1987**, *109*, 2009−2016.
(7) Oh, S. M.; Hendrickson, D. N.; Hassett, K. L.; Davis, R. E. *J. Am. Chem. Soc*. **1985**, *107*, 8009−8018.
(8) Sorai, M.; Kaji, K.; Hendrickson, D. N.; Oh, S. M. *J. Am. Chem. Soc*. **1986**, *108*, 702−708.
(9) Jang, H. G.; Kaji, K.; Sorai, M.; Wittebort, R. J.; Geib, S. J.; Rheingold, A. L.; Hendrickson, D. N. *Inorg. Chem*. **1990**, *29*, 3547−3556.
(10) Sorai, M.; Hendrickson, D. N. *Pure Appl. Chem*. **1991**, *63*, 1503−1510.
(11) Hendrickson, D. N. In *Mixed Valency Systems: Applications in Chemistry, Physics and Biology*; Prassides, K., Ed.; Kluwer Academic Publishers: Dordrecht, The Netherlands, 1991; pp 67−90.
(12) Cannon, R. D.; Jayasooriya, U. A.; arapKoske, S. K.; White, R. P.; Williams, J. H. *J. Am. Chem. Soc*. **1991**, *113*, 4158−4160.
(13) Wrobleski, J. T.; Dziobkowski, C. T.; Brown, D. B. *Inorg. Chem*. **1981**, *20*, 679−684.
(14) White, R. P.; Al-Basseet, J. O.; Cannon, R. D.; Kearley, G. J.; Jayasooriya, U. A. *Physica B* **1989**, 156−157, 367−369.
(15) Jayasooriya, U. A.; Cannon, R. D.; Anson, C. E.; arapKoske, S. K.; White, R. P.; Kearley, G. J. *J. Chem. Soc., Dalton Trans*. **1992**, 379−381.
(16) Cannon, R. D.; Jayasooriya, U. A.; White, R. P.; arapKoske, S. K. *Spectrochim. Acta* **1993**, *49A*, 1787−1791.
(17) Cannon, R. D.; Jayasooriya, U. A.; White, R. P. In *Mixed Valency Systems: Applications in Chemistry, Physics and Biology*; Prassides, K., Ed.; Kluwer Academic Publishers: Dordrecht, The Netherlands, 1991; pp 283−298.
(18) Oh, S. M.; Wilson, S. R.; Hendrickson, D. N.; Woehler, S. E.; Wittebort, R. J.; Inniss, D.; Strouse, C. E. *J. Am. Chem. Soc*. **1987**, *109*, 1073−1090.
(19) Ponomarev, V. I.; Filipenko, O. S.; Atovmian, L. O.; Bobkova, S. A.; Turte, K. I. *Dokl. Akad. Nauk. SSSR* **1982**, *262*, 346−350; *Sov. Phys. Dokl*. **1982**, *27*, 6.
(20) Ponomarev, V. I.; Turté, K. I.; Shilov, G. V.; Bobkova, S. A.; Atovmyan, L. O.; Stukan, R. A. *Koord. Khim*. **1986**, *12*, 398−403; *Sov. J. Coord. Chem*. **1986**, *12*, 241−246.
(21) Sorai, M.; Shiomi, Y.; Hendrickson, D. N.; Oh, S. M.; Kambara, T. *Inorg. Chem*. **1987**, *26*, 223−230.
(22) Poganiuch, P.; Liu, S.; Papaefthymiou, G. C.; Lippard, S. J. *J. Am. Chem. Soc*. **1991**, *113*, 4645−4651.
(23) Turte, K. I.; Bobkova, S. A.; Stukan, R. A.; Shova, S. G. *Koord. Khim*. **1981**, *7*, 1682−1691; *Sov. J. Coord. Chem*. **1981**, *7*, 841−849.

Table 1. Crystallographic Data for **1**, **2**, and **3**

	1	**2**		**3**	
	293 K	293 K	112 K	293 K	112 K
formula	$C_{12}H_{18}Br_6Fe_3O_{16}$	$C_{12}H_{28}Fe_3O_{18}$	$C_{12}H_{28}Fe_3O_{18}$	$C_{12}H_{24}Cl_6Fe_3O_{19}$	$C_{12}H_{24}Cl_6Fe_3O_{19}$
fw	1065.26	627.88	627.88	852.57	852.57
crystal system	monoclinic	monoclinic	monoclinic	monoclinic	monoclinic
space group	$P2_1/n$	$C2/c$	$C2/c$	$P2_1/n$	$P2_1/n$
sys absence	$h0l$: $h+l=2n$ $0k0$: $k=2n$	hkl: $h+k=2n$ $h0l$: $l=2n$	hkl: $h+k=2n$ $h0l$: $l=2n$	$h0l$: $h+l=2n$ $0k0$: $k=2n$	$h0l$: $h+l=2n$ $0k0$: $k=2n$
a, Å	15.775(2)	27.081(5)	26.621(13)	14.846(1)	14.741(4)
b, Å	14.923(2)	13.810(2)	13.897(2)	14.463(2)	14.355(2)
c, Å	12.476(2)	15.337(6)	15.132(14)	14.036(1)	13.947(3)
β, deg	105.18(1)	123.29(2)	122.79(6)	100.329(5)	100.34(2)
V, Å^3	2834.6(6)	4794(2)	4706(6)	2965.1(5)	2903(3)
Z	4	8	8	4	4
d_{calc}, g/cm^3	2.50	1.74	1.77	1.91	1.95
crystal size, mm	0.43 × 0.4 × 0.36	0.58 × 0.32 × 0.22	0.42 × 0.16 × 0.09	0.54 × 0.29 × 0.11	0.58 × 0.31 × 0.22
μ(Mo Kα), cm^{-1}	99.6	18.7	19.0	20.7	21.1
scan method	$\omega-2\theta$	$\omega-2\theta$	$\omega-2\theta$	$\omega-2\theta$	$\omega-2\theta$
data collcn range (2θ)	2−50	2−50	2−55	2−50	2−55
total reflcns measd	5439	9173	5901	5677	7096
unique reflcns	4969	4211	5395	5204	6639
reflecns used[a]	2505	3211	2981	3513	5622
parameters refined	319	298	288	457	457
R[b]	0.080	0.047	0.070	0.034	0.031
R_w[c]	0.103	0.077	0.084	0.040	0.046
largest shift/esd	0.04	0.01	0.09	0.31	0.03
highest peak, e/A^3	1.29(26)	1.80(12)	1.8(2)	0.88(8)	0.98(11)
goodness of fit[d]	2.93	2.62	2.34	1.24	1.70

[a] $I_o > 3\sigma(I_o)$. [b] $R = \sum[||F_o| - |F_c||]/\sum|F_o|$. [c] $R_w = [\sum w(|F_o| - |F_c|)^2/\sum w|F_o|^2]^{1/2}$, $w = 1/\sigma^2|F_o|$. [d] Goodness of fit = $[\sum w(|F_o| - |F_c|)^2/$(no. of reflections − no. of parameters)$]^{1/2}$.

enriched metallic iron foil was used for velocity calibration. All the isomer shift values were described with respect to the metallic iron.

X-ray Structure Determination. For measurements at 293 K, crystals (**1**, **2**, and **3**) glued on top of a glass fiber were mounted in a glass capillary filled with nitrogen gas. In the case of chloroacetate crystal **3**, a small amount of water was added to the capillary in order to avoid the dehydration of crystal water. For complexes **2** and **3** crystal structures were also determined at 112 K. Crystals were glued and covered with grease inside a glass capillary and cooled with nitrogen gas to 112 K. Cell parameters were measured several times in the course of cooling to 112 K and there was no evidence of change in the crystal system. An Enraf-Nonius CAD4 diffractometer with a monochromated Mo Kα radiation source (0.71073 Å) was used for data collection. Intensities of equivalent reflections were averaged. Corrections were applied for Lorentz and polarization effects. Linear decay collection was applied to the data of **1**, **2**, and **3** obtained at 293 K. An empirical absorption correction based on a series of ψ-scans was applied to data of **1** (293 K), **2** (112 K), and **3** (293 and 112 K). Crystal data and experimental conditions are summarized in Table 1.

All calculations were done using the Enraf-Nonius package MolEN program on a VAX 3400 computer.[24] The structure was solved by the direct method (SIR 88).[25] All non-hydrogen atoms were located by using alternating cycles of least-squares refinements and difference Fourier synthesis, and their positions and anisotropic thermal parameters were refined using full-matrix least squares. Hydrogen atoms were located only for the chloroacetate complex **3** (293 and 112 K) by successive difference Fourier syntheses, and their positions and isotropic thermal parameters were refined using full-matrix least squares.

Results and Discussion

^{57}Fe-Mössbauer Spectroscopy. Mössbauer spectra of $[Fe_3O(CH_2BrCO_2)_6(H_2O)_3]$ (**1**) measured at 82 and 296 K are shown in Figure 1. At both temperatures, the spectra are least-squares fitted by two sets of quadrupole-split doublets ascribed to an Fe^{II} state and an Fe^{III} state with a nearly 1:2 areal intensity ratio. The Mössbauer parameters are summarized in Table 2. The compound exhibits only a temperature-independent trapped-valence state at temperatures below 296 K. Temperature dependence of the Mössbauer spectral shape is mainly ascribed to the decrease in quadrupole splitting of the Fe^{II} doublet. This change is expected for an Fe^{II} high-spin compound and is no way related to valence delocalization.

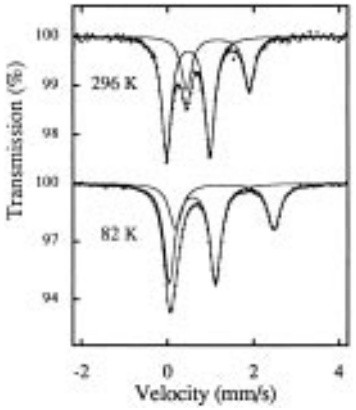

Figure 1. ^{57}Fe-Mössbauer spectra of $[Fe_3O(CH_2BrCO_2)_6(H_2O)_3]$ (**1**).

Table 2. Mössbauer Parameters for $[Fe_3O(CH_2BrCO_2)_6(H_2O)_3]$ (**1**)

	δ (mm/s)[a]		ΔE_Q (mm/s)[b]		Γ (mm/s)[c]		area (%)	
T/K	Fe^{II}	Fe^{III}	Fe^{II}	Fe^{III}	Fe^{II}	Fe^{III}	Fe^{II}	Fe^{III}
82	1.33	0.57	2.29	1.07	0.29	0.27	35.4	64.6
296	1.17	0.48	1.47	1.00	0.36	0.30	33.6	66.4

[a] Isomer shift relative to metallic iron. [b] Quadrupole splitting. [c] Full width at half-maximum.

Figure 2 shows Mössbauer spectra of $[Fe_3O(CH_3CO_2)_6(H_2O)_3]\cdot 2H_2O$ (**2**). There are several papers on Mössbauer spectroscopic measurements of this acetate−aqua complex which has zero or two crystal water molecules.[13,26,27] Temperature dependence of the spectral shape has been interpreted in terms of an increase in the rate of intramolecular electron transfer

(24) MolEN, An Interactive Structure Solution Procedure, Enraf-Nonius, Deift, The Netherlands, 1990.

(25) Burla, M. C.; Camalli, M.; Cascarano, G.; Giacovazzo, C.; Polidori, G.; Spagna, R.; Viterbo, D. *J. Appl. Crystallogr.* **1989**, *22*, 389−393.

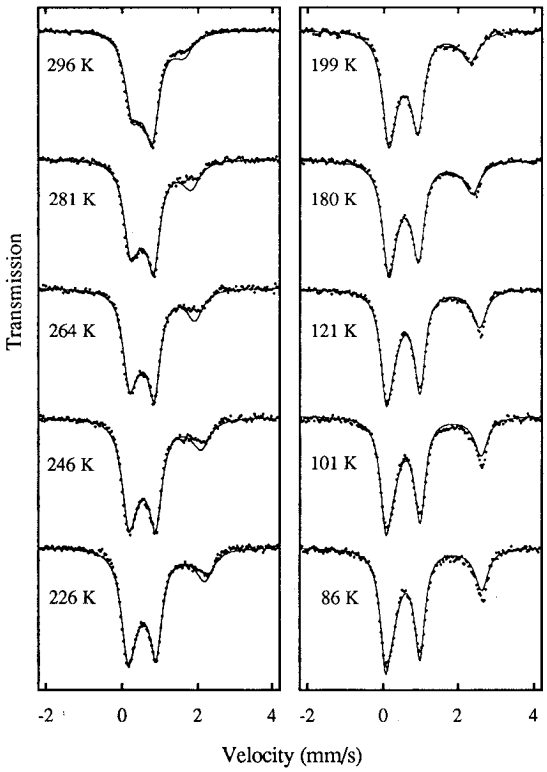

Figure 2. ^{57}Fe-Mössbauer spectra of $[Fe_3O(CH_3CO_2)_6(H_2O)_3]\cdot 2H_2O$ (**2**). Solid lines represent the simulated results obtained by the three-site relaxation model.

among the three iron atoms with increasing temperature. Wrobleski et al. have simulated the spectra by applying a three-site relaxation model modified from Wickmann's formula, in order to estimate intramolecular electron transfer rates for the nonhydrated complex.[13] They assumed relaxation processes between Fe^{II} and Fe^{III} nuclear energy levels with relaxation time τ and between Fe^{III} nuclear energy levels with relaxation time τ'. Following their procedure, we attempt to simulate Mössbauer spectra of the dihydrated complex **2** using the three-site relaxation model. The equation used in this study is essentially the same as that in Wrobleski et al.'s study but we neglected the relaxation process between Fe^{III} sites which negligibly affects the simulated results. The relaxation time τ is represented by $\tau = (\tau_{23}\tau_{32})/(\tau_{23} + \tau_{32})$ where τ_{23} and τ_{32} stand for the relaxation times for Fe^{II} to Fe^{III} and for Fe^{III} to Fe^{II}, respectively. The relative probability for Fe^{II} (P_{II}) is fixed at 0.333 which gives the relation of $P_{II} = \tau/\tau_{32}$. It is necessary to assume opposite signs for the quadrupole interaction in Fe^{II} and Fe^{III} sites and to leave isomer shift and quadrupole-split values adjustable. The simulated results are represented by solid lines in Figure 2 and fitting parameters are listed in Table 3. A discussion will be made regarding the crystal structure of **2**.

Black crystals of $[Fe_3O(CH_2ClCO_2)_6(H_2O)_3]\cdot 3H_2O$ (**3**) turn into red powders of $[Fe_3O(CH_2ClCO_2)_6(H_2O)_3]$ (**4**) due to loss of all three crystal water molecules when kept in air at ambient temperature. Since the X-ray powder patterns of compounds **3** and **4** are similar, it is concluded that no marked structural change occurs upon dehydration. A large difference is observed, however, between their Mössbauer spectra. Mössbauer spectra of the dehydrated complex **4** show a temperature-independent trapped-only valence state (Figure 3). Two sets of quadrupole-split doublets ascribed to Fe^{II} and Fe^{III} states with a nearly 1:2

(26) Lupe, D.; Barb, D.; Filoti, G.; Morariu, M.; Tarina, D. *J. Inorg. Nucle. Chem.* **1972**, *34*, 2803−2810.

(27) Gol'danskii, V. I.; Alekseev, V. P.; Stukan, R. A.; Turte, K. I.; Ablov, A. V. *Dokl. Akad. Nauk. SSSR* **1973**, *213*, 867−870.

Table 3. Mössbauer Fitting Parameters Used for the Simulation[a]

	δ (mm/s)		ΔE_Q (mm/s)		
T/K	Fe^{II}	Fe^{III}	Fe^{II}	Fe^{III}	τ (ns)
86	1.44	0.52	2.40	0.94	55.0
101	1.43	0.52	2.38	0.94	51.4
121	1.41	0.52	2.34	0.93	48.8
140	1.37	0.53	2.30	0.92	38.7
159	1.33	0.53	2.25	0.90	36.4
180	1.30	0.53	2.19	0.85	33.2
199	1.26	0.53	2.17	0.84	26.3
208	1.25	0.53	2.09	0.83	27.1
226	1.23	0.53	1.95	0.80	27.5
246	1.19	0.54	1.83	0.78	24.4
254	1.15	0.54	1.71	0.77	23.9
264	1.15	0.54	1.59	0.72	29.0
271	1.14	0.54	1.55	0.71	27.5
281	1.10	0.54	1.49	0.69	24.9
296	1.01	0.55	1.31	0.65	19.9

[a] Full width at half-maximum was assumed to be temperature independent and was fixed at 0.26 mm/s.

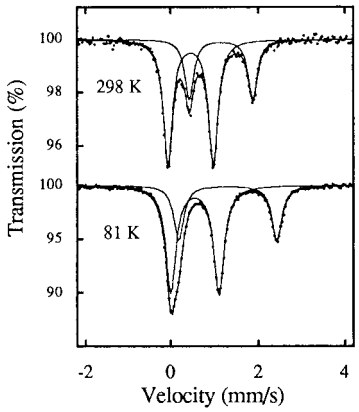

Figure 3. ^{57}Fe-Mössbauer spectra of $[Fe_3O(CH_2ClCO_2)_6(H_2O)_3]$ (**4**).

areal intensity ratio are found at 81 and 298 K. Figure 4 shows Mössbauer spectra of the hydrated complex **3**. It is found in the spectrum measured at 86 K that the central absorption of around 1 mm/s is decomposed into two lines ascribed to higher-velocity components of two distinct Fe^{III} quadrupole-split doublets. The spectrum is least-squares-fitted by three sets of quadrupole-split doublets, one ascribed to an Fe^{II} and two to Fe^{IIIA} and Fe^{IIIB} states. The Mössbauer parameters for **3** and **4** are summarized in Table 4.

As the temperature is increased, the Fe^{II} and Fe^{IIIA} doublets of **3** converge, while the Fe^{IIIB} doublet shows no significant temperature dependence. At 86 K the Fe^{IIIA} doublet shows larger quadrupole splitting than the Fe^{IIIB} doublet. It is found that the quadrupole splitting of the Fe^{IIIA} doublet is decreased with increasing temperature, while the Fe^{IIIB} doublet remains unchanged and the two Fe^{III} doublets become similar at 186 K. As the temperature is increased above 186 K the lower-velocity-component lines in each Fe^{III} doublet separate from each other, while the higher-velocity-component lines in each Fe^{III} doublet remain close to each other, indicating an increase in the isomer shift and a decrease in the quadrupole splitting of the Fe^{IIIA} doublet. Temperature dependence of the Fe^{II} doublet for the hydrated complex **3** is also different from that of the Fe^{II} doublet for the dehydrated complex **4**. The hydrated complex **3** shows a more pronounced decrease in quadrupole splitting and isomer shift. The spectral changes can be explained by assuming valence delocalization only over the two iron centers (Fe^{II} and Fe^{IIIA}).

There is no appreciable line broadening on the valence delocalization between Fe^{II} and Fe^{IIIA} doublets for **3**. Although

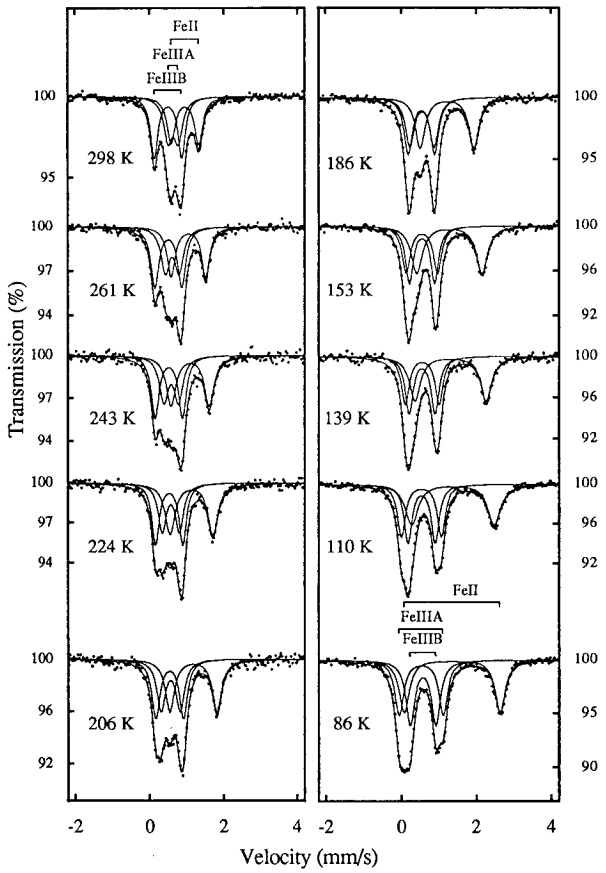

Figure 4. ^{57}Fe-Mössbauer spectra of $[Fe_3O(CH_2ClCO_2)_6(H_2O)_3]\cdot 3H_2O$ (**3**).

the Fe^{IIIB} doublet remains unchanged, the Fe^{II} and Fe^{IIIA} doublets show a temperature dependence similar to that observed in several biferrocenium salts.[28−33] In the biferrocenium salts, quadrupole-split doublets of ferrocene-like Fe^{II} and ferrocenium-like Fe^{III} converge with increasing temperature without appreciable line broadening, and finally become only one doublet ascribed to an averaged-valence state. The only example of an oxo-centered trinuclear iron carboxylate complex which was reported to show a similar temperature dependence of its Mössbauer spectrum is the acetate−4-ethylpyridine complex, $[Fe_3O(CH_3CO_2)_6(4\text{-Etpy})_3]\cdot 4\text{-Etpy}$.[7] The Mössbauer spectrum of the complex is decomposed into two sets of quadrupole-split doublets ascribed to an Fe^{II} state and an Fe^{III} state at low temperature. Although only one Fe^{III} doublet is observed in the acetate−4-ethylpyridine complex, the Fe^{II} and Fe^{III} doublets converge without appreciable line broadening with increasing temperature.

X-ray Crystallography. The molecular structure of the bromoacetate complex **1** determined at 293 K is shown in Figure 5. The compound is crystallized in space group $P2_1/n$. There is no crystallographically imposed symmetry. Selected bond distances and angles are listed in Table 5. The central O4 atom is placed on the plane defined by the three iron atoms within the estimated standard deviation (O4 indicates a central oxygen atom in this study). The central Fe_3O atoms form nearly an isosceles triangle array (one long and two short distances and one large and two small angles). Fe3−O4 (2.00(1) Å) is longer than Fe1−O4 and Fe2−O4 by 0.14 and 0.17 Å, respectively, Fe1−O4−Fe2 (124.3(6)°) is larger than Fe1−O4−Fe3 and Fe2−O4−Fe3 by 6.0° and 6.9°, respectively. The averaged distance between the Fe3 atom and coordinated six oxygen atoms, $Fe3-O_{av}$, is also longer than $Fe1-O_{av}$ and $Fe2-O_{av}$ by 0.09 Å. The $O4-Fe-O_{carbox}$ angles (averaged angle of the four bonds constructed by O4, Fe, and an oxygen atom from carboxylate ligands) also depend on the valence states. The $O4-Fe3-O_{carbox}$ angle is smaller than those of the other two iron atom sites. The distances of the Fe−O4 bond and the angles of $O4-Fe-O_{carbox}$ seem to strongly depend on the valence states. The structural data are consistent with the above Mössbauer result which shows a trapped-valence state at 296 K. It is concluded that the Fe1 and Fe2 atoms are in an Fe(III) state and that the Fe3 atom is in an Fe(II) state. Although the coordination geometries of Fe1 and Fe2 are slightly different, separated Fe^{III} quadrupole-split doublets are not resolved. The single Lorentzian line doublet seems to fit well even without assuming an additional Fe^{III} doublet.

The acetate complex **2** is crystallized in space group $C2/c$ at 293 and 112 K. The compound consists of one $[Fe_3O(CH_3CO_2)_6(H_2O)_3]$ molecule and two crystal water molecules. There is no crystallographically imposed symmetry. The structure of the $[Fe_3O(CH_3CO_2)_6(H_2O)_3]$ molecule at 293 K is shown in Figure 6. Selected bond distances and angles at 112 and 293 K are listed in Table 6. The two crystal water molecules are located along the *c*-axis with distances between their oxygen atoms (O21 and O22) of 3.09(3) and 4.81(3) Å at 293 K (3.85(6) and 4.59(4) Å at 112 K) (see Figures 7 and 8). The $[Fe_3O(CH_3CO_2)_6(H_2O)_3]$ molecule sits around the crystal water and the Fe3 atom site is close to the crystal water molecules. The O21 is located near O8 and O3 separated by 2.87(1) and 2.96(1) Å at 293 K (3.13 (3) and 3.31(2) Å at 112 K), respectively, and the O22 atom is located near the O3, O9, and O15 atoms separated by 3.29(2), 3.40(1), and 3.24(1) Å at 293 K (2.974(4), 3.45(2), and 3.37(3) Å at 112 K), respectively. The central O4 atom is approximately located on the Fe_3 plane (0.007(3) Å at 293 K and 0.001(5) Å at 112 K). The coordination geometries of the three iron atoms show better equivalence than those in **1**, but slight differences are still observed (for example, 0.039 Å between Fe1−O4 and Fe3−O4 at 293 K). It is also found that the Fe1−O4 bond is the shortest and the Fe3−O4 bond is the longest at 293 K, while the Fe3−O4 bond is the shortest and the Fe2−O4 bond is the longest at 112 K. Such inequivalencies may limit the application of the three-site relaxation model used for the simulation of the Mössbauer spectra. The relaxation model assumes the same relaxation time τ for each pair of Fe^{II} and Fe^{III} atoms. This assumption is rigorously applicable only when the three iron atoms are in an equivalent chemical environment. In Figure 2, the disagreement between the simulated lines and experimental data is appreciable around the shoulder at 1∼2 mm/s above 226 K. Although better fitting results of the simulation can be achieved by using three different quadrupole-split doublets for the Fe^{II} state and three different τ_{23} and τ_{32}, we cannot estimate a plausible correlation among these new adjustable parameters. On the other hand, we attempted a Lorentzian line analysis without consideration of the relaxation effect for the 86 K spectrum; however, no good fit was obtained when we adopted only one quadrupole-split doublet each for the Fe^{III} component and the Fe^{II} component. The peaks observed in the spectrum measured at 86 K are rather

(28) Nakashima, S. *Nucl. Inst. Methods Phys. Res.* **1993**, *B76*, 408−414.
(29) Sano, H. *Hyperfine Interactions* **1990**, *53*, 97−112.
(30) Iijima, A.; Saida, R.; Motoyama, I.; Sano, H. *Bull. Chem. Soc. Jpn.* **1981**, *54*, 1375−1379.
(31) Dong, T.-Y.; Hendrickson, D. N.; Iwai, K.; Cohn, M. J.; Geib, S. J.; Rheingold, A. L.; Sano, H.; Motoyama, I.; Nakashima, S. *J. Am. Chem. Soc.* **1985**, *107*, 7996−8008.
(32) Nakashima, S.; Katada, M.; Motoyama, I.; Sano, H. *Bull. Chem. Soc. Jpn.* **1986**, *59*, 2923−2925.
(33) Nakashima, S.; Masuda, Y.; Motoyama, I.; Sano, H. *Bull. Chem. Soc. Jpn.* **1987**, *60*, 1673−1680.

Table 4. Mössbauer Parameters for $[Fe_3O(CH_2ClCO_2)_6(H_2O)_3]$ (**4**) and $[Fe_3O(CH_2ClCO_2)_6(H_2O)_3]\cdot 3H_2O$ (**3**)

$[Fe_3O(CH_2ClCO_2)_6(H_2O)_3]$ (**4**)

	δ (mm/s)		ΔE_Q (mm/s)		Γ (mm/s)		area (%)	
T/K	Fe^{II}	Fe^{III}	Fe^{II}	Fe^{III}	Fe^{II}	Fe^{III}	Fe^{II}	Fe^{III}
81	1.31	0.56	2.23	1.10	0.28	0.28	33.7	66.3
298	1.16	0.47	1.44	1.04	0.25	0.26	32.2	67.8

$[Fe_3O(CH_2ClCO_2)_6(H_2O)_3]\cdot 3H_2O$ (**3**)

	δ (mm/s)			ΔE_Q (mm/s)			Γ (mm/s)			area (%)		
T/K	Fe^{II}	Fe^{IIIA}	Fe^{IIIB}	Fe^{II}	Fe^{IIIA}	Fe^{IIIB}	Fe^{II}	Fe^{IIIA}	Fe^{IIIB}	Fe^{II}	Fe^{IIIA}	Fe^{IIIB}
86	1.35	0.52	0.57	2.57	1.17	0.69	0.32	0.28	0.28	33.7	30.8	35.5
110	1.37	0.53	0.53	2.21	1.06	0.73	0.42	0.25	0.25	38.0	29.7	32.3
139	1.31	0.55	0.54	1.91	0.90	0.70	0.36	0.24	0.25	38.3	28.0	33.7
153	1.28	0.54	0.54	1.75	0.84	0.68	0.36	0.26	0.24	40.0	28.3	31.7
186	1.22	0.55	0.53	1.43	0.65	0.71	0.31	0.28	0.26	36.3	30.3	33.4
206	1.17	0.55	0.53	1.28	0.52	0.74	0.29	0.27	0.25	35.6	30.6	33.8
224	1.12	0.56	0.52	1.16	0.47	0.73	0.33	0.25	0.23	39.0	28.2	32.8
243	1.08	0.57	0.51	1.03	0.40	0.73	0.33	0.25	0.23	39.0	28.2	32.8
261	1.04	0.60	0.50	0.93	0.37	0.72	0.26	0.27	0.25	32.7	29.6	37.7
298	0.95	0.63	0.49	0.74	0.27	0.74	0.27	0.27	0.23	33.1	29.8	37.1

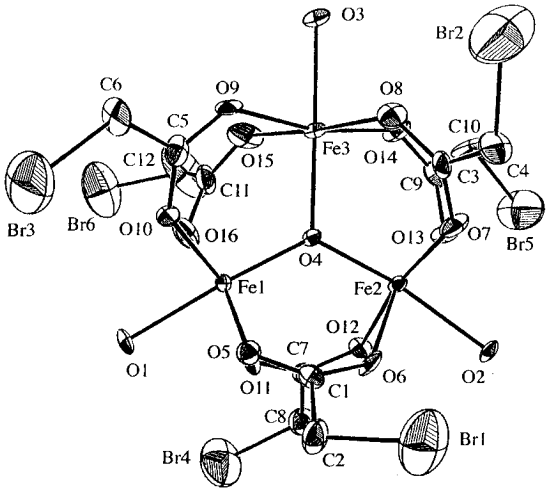

Figure 5. $[Fe_3O(CH_2BrCO_2)_6(H_2O)_3]$ (**1**) at 293 K with 50% probability of thermal ellipsoids.

Table 5. Selected Bond Distances (Å) and Angles (deg) for $[Fe_3O(CH_2BrCO_2)_6(H_2O)_3]$ (**1**) at 293 K

Distances					
Fe1−O4	1.86(1)	Fe2−O4	1.83(1)	Fe3−O4	2.00(1)
Fe1−O1	2.13(1)	Fe2−O2	2.12(1)	Fe3−O3	2.15(1)
$Fe1-O_{carbox}$[a]	2.04	$Fe2-O_{carbox}$[a]	2.04	$Fe3-O_{carbox}$[a]	2.12
$Fe1-O_{av}$[b]	2.02	$Fe2-O_{av}$[b]	2.02	$Fe3-O_{av}$[b]	2.11

Angles			
Fe1−O4−Fe2	124.3(6)	$O4-Fe1-O_{carbox}$[c]	96.4
Fe1−O4−Fe3	118.3(7)	$O4-Fe2-O_{carbox}$[c]	96.8
Fe2−O4−Fe3	117.4(6)	$O4-Fe3-O_{carbox}$[c]	93.8

[a] Averaged distances between iron and four oxygen atoms from carboxylate ligands. [b] Averaged distances between iron and coordinated six oxygen atoms. [c] Averages of four angles constructed by O4, Fe, and four oxygen atoms from carboxylate ligands.

broad compared with those observed in the spectrum for other compounds in this study. Therefore, it seems reasonable to conclude that the spectrum at 86 K is broadened by the relaxation effect due to the electron transfer.

Wrobleski et al. have determined the activation energy to be 0.06 eV for the electron transfer by applying the Arrhenius law.[13] The electron transfer rate ($1/\tau$) was assumed to be the rate constant of the following reaction.

$$Fe^{II}Fe^{III}Fe^{III} \overset{(1/\tau)}{\rightleftharpoons} Fe^{III}Fe^{II}Fe^{III}$$

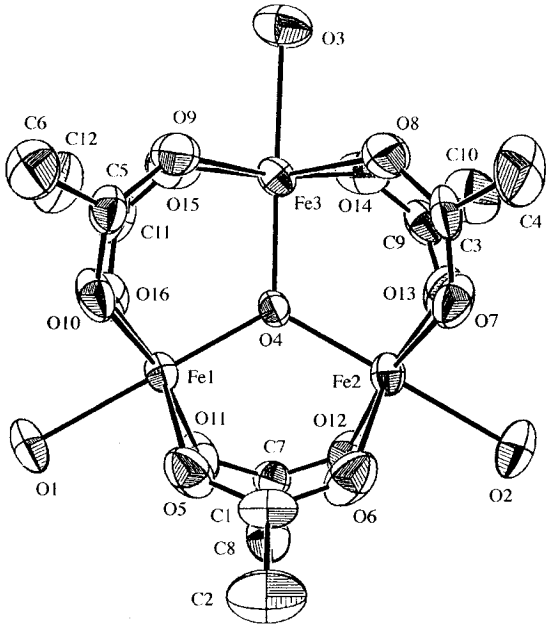

Figure 6. $[Fe_3O(CH_3CO_2)_6(H_2O_3)]$ in **2** at 293 K with 50% probability of thermal ellipsoids.

Following their procedure, we evaluated the activation energy to be 0.01 eV for the electron transfer. The acetate−aqua complex used in this study contains two crystal water molecules, while the previous experiment was performed on the nonhydrated complex. Although the crystal water molecules exhibit large thermal motion, interaction with the crystal water molecules may exert some effect on the rate of electron transfer.

The chloroacetate complex **3** is crystallized in $P2_1/n$ at 293 K. The compound consists of one $[Fe_3O(CH_2ClCO_2)_6(H_2O)_3]$ molecule and three crystal water molecules. There is no crystallographically imposed symmetry. Figure 9 shows the molecular structure of **3** at 293 and 112 K. The three crystal water molecules are separately located near each ligand water molecule at distances between the oxygen atoms of 2.660(5) (O1 and O21), 3.180(5) (O2 and O22), and 2.653(5) Å (O3 and O23) at 293 K and 2.658(3), 3.185(3), and 2.649(3) Å at 112 K, respectively. The central O4 atom is approximately located on the Fe_3 plane (0.020(3) Å at 293 K and 0.024(2) Å at 112 K). Table 7 shows selected bond distances and angles. The coordination geometry of the Fe3 atom is of the Fe(III) type. The Fe3−O4 and $Fe3-O_{av}$ distances, and the O4−Fe3−

Table 6. Selected Bond Distances (Å) and Angles (deg) for $[Fe_3O(CH_3CO_2)_6(H_2O)_3]\cdot 2H_2O$ (**2**) at 293 and 112 K

	293 K	112 K
	Distances	
Fe1−O4	1.867(4)	1.894(7)
Fe1−O1	2.161(5)	2.110(9)
Fe1−O_{carbox}	2.036	2.028
Fe1−O_{av}	2.029	2.019
Fe2−O4	1.904(4)	1.924(6)
Fe2−O2	2.143(5)	2.121(8)
Fe2−O_{carbox}	2.053	2.060
Fe2−O_{av}	2.043	2.047
Fe3−O4	1.906(4)	1.871(6)
Fe3−O3	2.181(5)	2.103(8)
Fe3−O_{carbox}	2.059	2.026
Fe3−O_{av}	2.054	2.013
	Angles	
Fe1−O4−Fe2	120.5(2)	119.1(3)
Fe1−O4−Fe3	120.0(2)	120.8(3)
Fe2−O4−Fe3	119.5(2)	120.1(3)
O4−Fe1−O_{carbox}	96.1	95.4
O4−Fe2−O_{carbox}	95.1	94.4
O4−Fe3−O_{carbox}	95.7	95.9

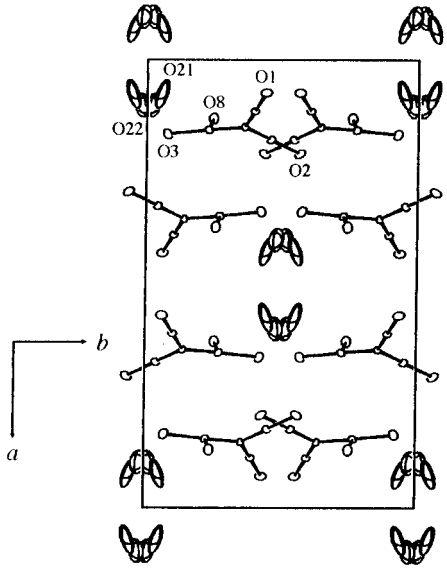

Figure 7. A projection of the crystal structure of **2** at 293 K along the *c*-axis. Crystal water molecules are drawn with principal axes of thermal motion. Acetate ligands except for the O8 atom are omitted for clarity.

O_{carbox} angle are nearly the same as those of Fe(III)-type atoms (Fe1 and Fe2) in complex **1**. These results indicate that the Fe3 atom corresponds to the Fe^{IIIB} atom shown by Mössbauer spectroscopy and the Fe1 and Fe2 atoms correspond to the iron atoms in valence delocalization. A significant change in the coordination geometry occurs in Fe1 and Fe2 sites when the crystal is cooled to 112 K, while the dimensions of the Fe3 site remain almost unchanged. The Fe_3O atoms array in the form of an isosceles triangle, 2.003(2) (Fe1−O4), 1.853(2) (Fe2−O4), and 1.849(2) Å (Fe3−O4). These distances and the other dimensions are comparable to those for the bromoacetate complex **1**. The X-ray structural data show good agreement with Mössbauer spectroscopic data, indicating valence delocalization over Fe1 and Fe2 atoms, but the valence states of Fe1 and Fe2 seem not to be completely averaged. Mössbauer components of Fe^{II} and Fe^{IIIA} remain distinct at 298 K, and the Fe1−O4 bond distance is 0.062 Å longer than Fe2−O4. If the valencies are completely averaged between the two atoms, a bond distance of 1.928 Å, (2.003 Å + 1.853 Å)/2, would be

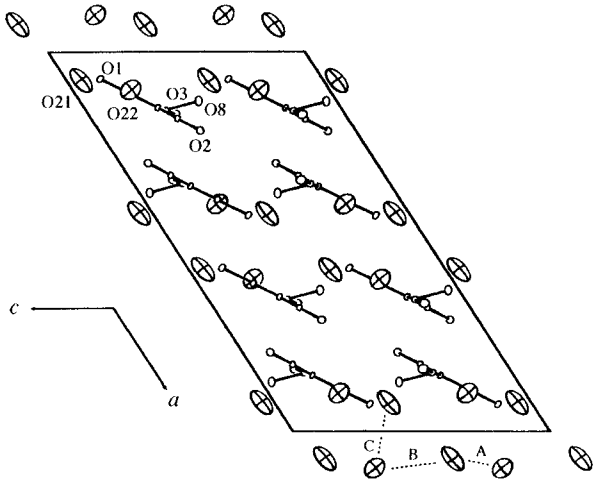

Figure 8. A projection of the crystal structure of **2** at 293 K along the *b*-axis. Crystal water molecules are drawn with principal axes of thermal motion. Acetate ligands except for the O8 atom are omitted for clarity. $A = 3.09(3)$ Å, $B = 4.81(3)$ Å, and $C = 4.04(2)$ Å.

expected for an Fe(II−III) averaged atom. The Fe1−O4 bond distance (1.957(3) Å) at 293 K is estimated to be an intermediate value between Fe(II) and Fe(II−III), whereas the Fe2−O4 bond distance (1.895(3) Å) is estimated to be an intermediate value between Fe(III) and Fe(II−III).

Recently Nakamoto et al. reported that the hydrogen bond plays an important role in valence delocalization in the iron cyanoacetate complex $[Fe_3O(CH_2CNCO_2)_6(H_2O)_3]$, which has a crystallographically imposed C_3 molecular symmetry.[5] The H_2O ligands and nitrogen atoms from neighboring molecules form a three-dimensional intermolecular hydrogen-bonding network at room temperature. The Mössbauer spectra of $[Fe_3O(CH_2CNCO_2)_6(H_2O)_3]$ show a sudden conversion from a trapped-valence state to an averaged-valence state within a 10 K range. There obviously exists strong intermolecular interaction in the hydrogen-bonding network associated with the valence state conversion. In the chloroacetate complex **3**, a calculation of intra- and intermolecular distances between oxygen atoms within 3.0 Å gives a possibility of the five hydrogen bonds listed in Table 8. Although an intermolecular hydrogen-bonding network O3−H6··O23−H12··O21··H2−O1 with O2−H4··O6 found in **3** is expected to show an intermolecular interaction that is not strong enough to cause an abrupt conversion of the valence states, the intra- and intermolecular hydrogen bonds may induce a change in the electronic states. Since the Mössbauer spectra of the dehydrated chloroacetate complex **4** do not show the two distinct Fe^{III} doublets, it is expected that the (O3)H6··O23 hydrogen bond affects the local environment around the Fe3 (Fe^{IIIB}) atom and stabilizes the Fe3 atom in a Fe^{III} state, causing a smaller electric field gradient. It is found that the Fe3−O3 bond is slightly extended. The Fe3−O3 bond distance is 0.028 and 0.041 Å longer at 293 K (0.027 and 0.037 Å at 112 K) than both the Fe1−O1 and Fe2−O2 distances, respectively. Another hydrogen bond between a ligand water molecule and a crystal water molecule, (O1)H2··O21, is formed at the Fe1 site, which has nearly the same bond angle and distance as those of the (O3)H6··O23 hydrogen bond, although the Fe1 atom is involved in valence delocalization. The O21 atom is displaced by −2.453(4) Å from the plane defined by the three iron atoms with the Fe1−O1··-O21 angle of 102.0(1)°. The O23 atom is displaced by 1.396-(4) Å from the Fe_3 plane with the Fe3−O3··O23 angle of 121.4(2)°. The O21 atom is included in one other hydrogen bond (H12··O21), while the O23 atom is included in two other hydrogen bonds (H11··O22 and H12··O21).

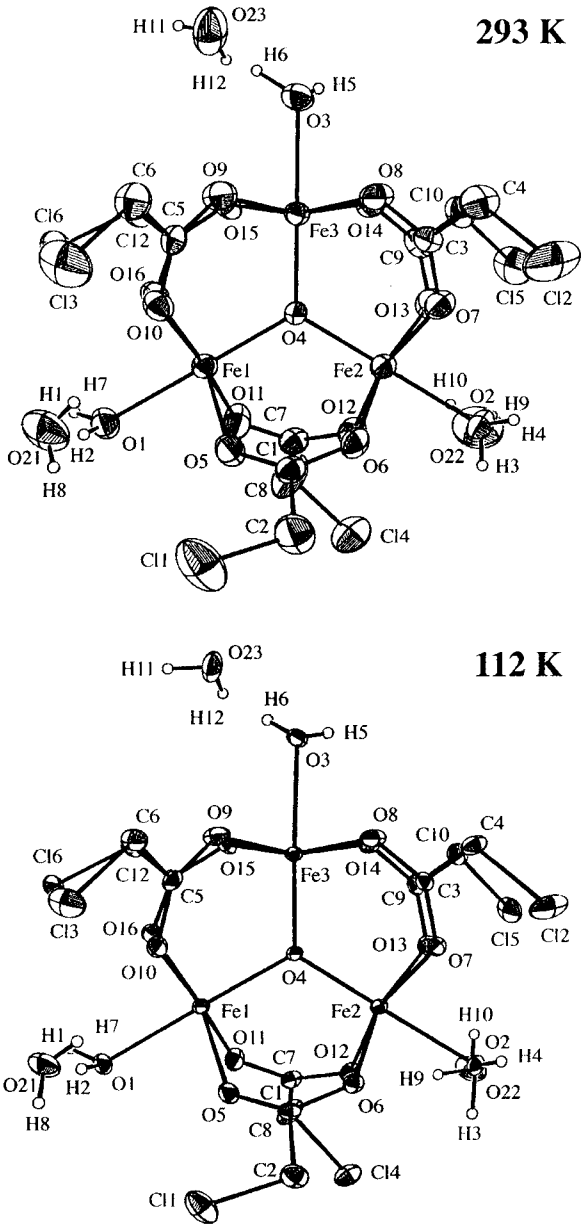

Figure 9. $[Fe_3O(CH_2ClCO_2)_6(H_2O)_3]\cdot 3H_2O$ (**3**) at 293 and 112 K showing 50% probability of thermal ellipsoids for non-hydrogen atoms. Hydrogen atoms of chloroacetate ligands are omitted for clarity. The three crystal water molecules are each located close to the nearest ligand water molecule.

As seen in Figure 4, Fe^{II} and Fe^{IIIA} components converge without appreciable line broadening, as observed in several biferrocenium salts. It is clear that the temperature dependence cannot be simply interpreted by assuming electron hopping over a finite activation energy with rate comparable to the Mössbauer time scale. It is impossible to simulate the spectra by the three-site relaxation model. There should be a significant change in the potential-energy surface to change electronic coupling, vibrational coupling, and/or a zero-point energy difference between vibronic states. The spectral change can be explained by assuming populational differences between $[Fe1^{II}Fe2^{III}Fe3^{III}]$ and $[Fe1^{III}Fe2^{II}Fe3^{III}]$ states and intramolecular electron transfer rates that are much faster than the Mössbauer time scale, as suggested by Masuda and Sano to account for the spectral change in the biferrocenium salts.[34] It is necessary to assume electron transfer rates to be much faster than the Mössbauer time scale in order to account for the absence of line broadening.

(34) Masuda, Y.; Sano, H. *Bull. Chem. Soc. Jpn.* **1987**, *60*, 2674−2676.

Table 7. Selected Bond Distances (Å) and Angles (deg) for $[Fe_3O(CH_2ClCO_2)_6(H_2O)_3]\cdot 3H_2O$ (**3**) at 293 and 112 K

	293 K	112 K
	Distances	
Fe1−O4	1.957(3)	2.003(2)
Fe1−O1	2.125(3)	2.115(2)
$Fe1-O_{carbox}$	2.092	2.116
$Fe1-O_{av}$	2.075	2.097
Fe2−O4	1.895(3)	1.853(2)
Fe2−O2	2.112(3)	2.105(2)
$Fe2-O_{carbox}$	2.074	2.060
$Fe2-O_{av}$	2.051	2.033
Fe3−O4	1.846(3)	1.849(2)
Fe3−O3	2.153(3)	2.142(2)
$Fe3-O_{carbox}$	2.023	2.021
$Fe3-O_{av}$	2.015	2.012
	Angles	
Fe1−O4−Fe2	118.4(1)	118.36(9)
Fe1−O4−Fe3	120.3(1)	118.68(9)
Fe2−O4−Fe3	121.3(1)	122.91(9)
$O4-Fe1-O_{carbox}$	94.5	93.59
$O4-Fe2-O_{carbox}$	95.9	96.92
$O4-Fe3-O_{carbox}$	97.0	96.84

Table 8. Interatomic Distances (Å) and Angles (deg) Involved in Hydrogen Bonds in $[Fe_3O(CH_2ClCO_2)_6(H_2O)_3]\cdot 3H_2O$ (**3**) at 293 and 112 K

	293 K	112 K
	Distances	
O1···O21	2.660(5)	2.658(3)
H2···O21	1.91(4)	1.86(4)
O2···O6	2.772(4)	2.757(3)
H4···O6[a]	1.98(6)	2.08(5)
O3···O23	2.653(5)	2.649(3)
H6···O23	1.63(6)	1.89(3)
O23···O21	2.855(6)	2.839(3)
H12···O21[b]	1.89(7)	2.09(4)
O23···O22	2.793(6)	2.752(3)
H11···O22[c]	2.21(5)	1.91(4)
	Angles	
O1−H2···O21	160(4)	168(4)
O2−H4···O6	168(6)	164(5)
O3−H6···O23	165(5)	168(3)
O23−H12···O21	159(6)	163(4)
O23−H11···O22	158(6)	170(4)

[a,b,c] Intermolecular hydrogen bonds. Symmetry codes: (a, O6) $-x+1, -y+1, -z$; (b, O21) $x-\frac{1}{2}, -y+\frac{1}{2}, z-\frac{1}{2}$; (c, O22) $x-\frac{1}{2}, -y+\frac{1}{2}, z+\frac{1}{2}$. An O3 atom is connected to the Fe1 site of the neighboring molecule along the *n*-glide plane by a network of O3−H6···O23−H12···O21···H2−O1, making a one-dimensional molecular chain, while the O2−H4···O6 hydrogen bond forms a dimer via the center of inversion.

The thermal populations for the $[Fe1^{II}Fe2^{III}Fe3^{III}]$ and $[Fe1^{III}Fe2^{II}Fe3^{III}]$ states are expected to correspond to the potential-energy difference between the two states and to be reflected in the crystal structure in which the Fe1 atom is in an intermediate state between Fe^{II} and Fe^{II-III} and the Fe2 atom is in an intermediate state between Fe^{III} and Fe^{II-III}.

Conclusion

The chloroacetate complex **3** is the first example of an oxo-centered mixed-valence trinuclear iron carboxylate complex where two distinct Fe^{III} sites are observed by Mössbauer spectroscopy, as well as the first example in which valence delocalization only between two iron atoms is observed. The valence states of each iron atom in **3** were defined by comparing the Mössbauer data and crystal structure of **3** with those of the bromoacetate complex **1** and the acetate complex **2**. The

Mössbauer and structural data of complex **1** indicate that it is in a trapped-valence state. On the other hand, the three-site relaxation model assuming an electron-hopping process was used to interpret the temperature dependence of the Mössbauer spectra of **2**. The simulated result is consistent with the crystal structure which shows better equivalence among the iron sites than that in complex **1**. Comparison of the Mössbauer spectra of the trihydrated chloroacetate complex **3** and the dehydrated chloroacetate complex **4** indicates that the electronic states of the chloroacetate complex **3** are strongly affected by the presence of crystal water. The X-ray crystal structure of **3** shows the presence of hydrogen bonds involving crystal water molecules and coordinated water molecules. It is suggested that the (O3)H6··O23 hydrogen bond affects the local environment of the Fe3 atom and causes a small electric field gradient. Mössbauer spectra of **3** show that the Fe^{II} and Fe^{IIIA} components converge without appreciable line broadening. The temperature dependence cannot be interpreted by the electron-hopping mechanism, which is applied to the case of the acetate complex **2**. Intermolecular hydrogen-bonding interaction is expected to induce a change in the potential-energy surface associated with valence delocalization. Although the intermolecular hydrogen bonds found in complex **3** are not strong enough to cause an abrupt conversion of the valence state, hydrogen-bonding intermolecular interaction is expected to play an important role in valence delocalization.

Acknowledgment. We thank Drs. Takao Matsuzaki, Yasuko Osano, and Yuko Kojima for their helpful suggestions in X-ray crystal structure analysis. We also express our thanks to Drs. Hideki Saito and Kimiko Kobayashi for their helpful suggestions in X-ray crystal structure analysis. We also thank Kiyomi Ishishita and Kei Sakauchi for their assistance in compound preparation.

Supporting Information Available: Tables of positional parameters, isotropic and anisotropic thermal parameters, bond distances, bond angles, and deviations (Å) of atoms from least-squares planes of **1** (293 K), **2** (293 and 112 K), and **3** (293 and 112 K) (36 pages). This material is contained in many libraries on microfiche, immediately follows this article in the microfilm version of the journal, can be ordered from the ACS, and can be downloaded from the Internet; see any current masthead page for ordering information and Internet access instructions.

JA953038Y